Magnon thermal mean free path in yttrium iron garnet

Stephen R. Boona[1] and Joseph P. Heremans[1,2]
[1]*Department of Mechanical and Aerospace Engineering, The Ohio State University, Columbus, Ohio 43210, USA*
[2]*Department of Physics, The Ohio State University, Columbus, Ohio 43210, USA*
(Received 2 July 2014; revised manuscript received 6 August 2014; published 22 August 2014)

The magnetothermal properties of monocrystalline yttrium iron garnet (YIG) are reported. The magnon contribution to both the thermal conductivity and specific heat at low temperatures has been determined by measuring these properties under an applied magnetic field, which allows us to freeze the magnon modes and isolate the phonon contribution relative to the zero-field behavior. These results are interpreted within the framework of a simple kinetic gas model for magnon heat conduction that allows us to estimate the magnon thermal mean free path, i.e., the inelastic scattering length scale for thermally driven bulk magnons. We observe this parameter to reach as high as approximately 100 μm at 2 K. It tracks the acoustic phonon thermal mean free path closely and decreases rapidly as the temperature is increased. This relatively short length scale suggests that magnon modes at thermal energies in YIG are not solely or directly responsible for coherent macroscale thermal spin transport (e.g., in the spin Seebeck effect) at high temperatures. Instead, these results support a growing consensus that subthermal magnons, i.e., those at energies below about 30 $\pm$ 10 K, are important for spin transport in YIG at all temperatures. These results also emphasize that magnon effects should be considered wavelength dependent, and that magnon-magnon interactions may be just as important for thermal spin transport as magnon-phonon scattering. This, in turn, has implications for understanding the characteristic temperature and length scales involved in spin caloritronic phenomena.

DOI: 10.1103/PhysRevB.90.064421 PACS number(s): 66.70.−f, 44.10.+i, 72.10.Di

I. INTRODUCTION

The rapidly expanding field of spin caloritronics [1,2] has generated a surge of interest in the magnetic and thermal properties of a wide variety of materials. Via processes such as the spin Seebeck (SSE) [3–5] and spin Peltier (SPE) [6] effects, as well as the (inverse [7]) spin Hall effect (SHE) [8,9], a bevy of spin-dependent transport mechanisms are now available for probing the magnetic, electronic, and thermal properties of various materials and heterostructures. The spin Seebeck effect has been reported in two clearly different geometries, the longitudinal SSE (LSSE), where magnon transport is parallel to the temperature gradient, and the transverse geometry (TSSE), where it is perpendicular. It was suggested, but not proven, that the TSSE can be viewed as a variation of LSSE with nonlocal spin detection. A key step in designing and interpreting experiments in this field lies in developing an appropriate understanding of the relevant interactions between the elementary excitations (magnons, phonons, and, in electrical conductors, spin-polarized electrons) whose fluxes govern spin transport, and the corresponding length scales over which these processes occur. For example, one important parameter is the distance over which coherent spin currents persist in various materials (the spin diffusion length), as this distance correlates with the limiting length scale of heterostructure components whose functions rely on spin transport [10].

In order to isolate and understand the nature of various possible interactions between fluxes of heat, charge, and magnetization in materials, it is convenient to examine materials in which only one or two of the relevant elementary excitations are active at a time. To study phonon-magnon interactions, for example, it is desirable to examine materials that have relatively large band gaps and high Curie temperatures, so that the material remains both electrically insulating and magnetically ordered within the desired temperature range of study. For these reasons, certain transition metal oxides, in particular yttrium iron garnet ($Y_3Fe_5O_{12}$, or YIG), have become ubiquitous in spin caloritronic experiments. This material has a band gap of approximately 2.85 eV [11]; its Curie (T_C = 550 K [12]) and Debye (T_D = 531 K, this work) temperatures are remarkably close to each other, and relatively high. The desired electronic and magnetic properties are thus easily maintained at room temperature and below. The absence of itinerant electrons in YIG means that the localized core d electrons of the iron atoms are the primary source of spin and magnetization dynamics in the material, and thermal energy then propagates through only perturbations of the magnetization (magnons) and/or real-space displacements of the atoms (phonons).

Experimental measurements [13] of the magnon dispersion in YIG by neutron diffraction, in addition to numerical simulations, report that the magnons can be reasonably well described by a quadratic dispersion:

$$\hbar\omega = Da^2k^2, \tag{1}$$

up to approximately ~620 GHz (30 K). Here a is the size of the unit cell (1.24 nm) and D corresponds to a spin-wave stiffness parameter measured in units of temperature ranging from about 46 K (for the limit where $a^2k^2 \rightarrow$ zero) to 35 K (when $a^2k^2 = 0.01$) [13]. Additional magnon modes appear in the dispersion near 620 GHz. An "optical-like" magnon mode appears near ~150 K, and this mode hybridizes with the "acousticlike" mode whose dispersion at this energy is approximately linear. The linearity of this latter mode allows for the calculation of a corresponding "pseudoacoustic" group velocity $v_M = d\omega/dk$, which is ~8500 m/s at these energies and temperatures.

The conceptual similarities between thermal magnons and phonons suggest that the relevant length scales that describe inelastic scattering for magnons should be similar to those of phonons. This implies that magnon spin currents may, under appropriate conditions, propagate significantly farther than electronic spin currents, which makes magnon-based materials an intriguing avenue for the possibility of developing spin-based devices with more practical dimensions. This idea is made more appealing when one considers that magnon currents may be efficiently excited via thermal processes (e.g., SSE), which typically occur at higher energies relative to electronic or resonant excitation methods. These higher energies in turn provide access to proportionately larger densities of spin states, and thus potentially larger spin current densities [14] and larger output voltages in spin-charge transducers. Although resonant excitations can also pump high magnon populations, this is true for only the states available at their specific energies.

The other key feature that makes YIG attractive for spin caloritronic experiments is the relative strength of phonon-magnon coupling. In general, magnons and phonons may exist at different effective temperatures in a material [15]. In the limiting case where magnon-phonon coupling is infinitely strong, the magnon and phonon baths are in local equilibrium everywhere at all times; the two can hybridize [16] or scatter resonantly [17], which is common in antiferromagnets. In that case, the driving force for SSE disappears, because thermal spin pumping depends on the existence of a temperature difference between the magnon bath in the ferromagnet and the electron bath in the normal metal; the latter is in equilibrium with the phonon baths, while the former is not. In the opposite extreme, where the coupling is zero, it becomes impossible to pump heat into or out of the magnon bath, and the magnons again contribute nothing to the thermal conductivity. The coupling strength in YIG lies in between these extremes, such that some heat is transferred between the magnon and phonon baths, but the coupling is not so strong that the magnon conductivity is quenched [15].

In spite of the widespread use of this material in spin caloritronic experiments, lingering questions remain regarding the length scales governing spin and heat transport. Recent reports have provided some insights into this problem, and we build upon those results here. Agrawal *et al.* have concluded via spatially resolved optothermal measurements near room temperature that short wavelength magnons cannot directly contribute to SSE in YIG [18], and Tikhonov *et al.* [19] have presented complementary calculations that indicate an important role for subthermal phonons (i.e., those of energies $<k_BT$, where T is the temperature of the measurements and k_B the Boltzmann constant) in SSE effects at room temperature. These results together suggest that subthermal magnons are indeed a critical feature that drives SSE. In addition to these studies, LSSE measurements performed at room temperature as a function of YIG film thickness show that the signal strength is strongly dependent on the film thickness up to $\sim$150 nm, beyond which the signal appears to saturate [20]. This latter result suggests that the LSSE relies heavily on processes that occur in the bulk of the YIG, and that it is not simply a surface effect at the YIG/Pt interface. It also suggests that 150 nm may correspond with the room temperature scattering length of the particular magnon modes responsible for LSSE. In contrast, the fact that transverse spin Seebeck signals are observed in YIG [21] over the entire macroscopic length of the sample, which can reach 1 cm and thus cannot be related to the above length scale, suggests that the TSSE is more complicated than LSSE. One important aspect to consider is that different magnon modes (e.g., long vs short wavelength, surface vs bulk modes, etc.) are affected by different scattering mechanisms with different scattering cross sections, and this may perhaps help reconcile the counterintuitive nature of macroscale spin transport in YIG [19,22].

The details of magnon-phonon scattering are important for bulk modes, and this scattering appears to be dependent on the temperature of the material as well as the specific phonon oscillation orientation (i.e., longitudinal vs transverse) and momentum state [23]. As opposed to the room temperature behavior, we expect the relevant mechanisms to be different at low temperatures where long wavelength modes constitute a larger percentage of the occupied modes. This corresponds to the regime in Ref. [23] where magnon-phonon coupling is still present, but relatively weak. Indeed, Uchida *et al.* observed very different low-temperature behavior in LSSE experiments on YIG|Pt heterostructures when comparing the signals generated from a monocrystalline YIG slab to those obtained from a polycrystalline sample, which they interpreted to be related to the suppression of phonon conductivity by boundary scattering in the latter case [24]. At temperatures above 100 K, however, the behaviors appear to converge, indicating that boundary scattering is not a significant mechanism behind the observed temperature dependence in the high-temperature limit.

To outline a framework in this paper within which we experimentally explore the length scale of bulk spin transport in YIG, we start from a model of magnon heat conduction that approximates the total thermal conductivity κ to be comprised of two independent contributions, one from magnons (κ_M), and one from phonons (κ_λ):

$$\kappa = \kappa_\lambda + \kappa_M. \tag{2}$$

This approximation is a quite aggressive simplification, since (as discussed above) a nonzero magnon-phonon coupling is necessary in order for magnons to contribute to the thermal conductivity. We nonetheless use (2) as a phenomenological framework to describe the effective contribution from each conduction channel. Since magnons and phonons are bosons with low population densities at low temperature ($T < T_D, T_C$), we apply the conventional kinetic gas theory to express their individual contributions to the thermal conductivity in terms of the standard relationship describing heat conduction in a diffusive system. Within this approximation, the thermal conductivity can be written as [25]

$$\kappa = \tfrac{1}{3} C_\lambda v_\lambda l_\lambda + \tfrac{1}{3} C_M v_M l_M, \tag{3}$$

where C is the isobaric specific heat per unit volume, v is the group velocity, l is the thermal mean free path (MFP), and the subscripts distinguish between the phonon (λ) and magnon (M) properties. Furthermore, we can define the magnon thermal conductivity by Fourier's law as the magnon heat current density ($j_{Q,M}$) divided by the magnon temperature

gradient ∇T_M,

$$\kappa_M = \frac{j_{Q,M}}{\nabla T_M}. \tag{4}$$

Equation (3) produces single estimates for the effective average MFP of all magnons (l_M) and all phonons (l_λ), rather than their frequency and mode-dependent values. Although this is obviously an oversimplification, this is a historical approach now known in phonon physics to nonetheless be a robust approximation applicable to many materials [26]. The analogy between phonon and magnon thermal transport further suggests that a calculation of l_M obtained within this framework will likely overemphasize the contributions of higher-energy thermal magnons with short MFP, and that a non-negligible flux of magnons with energies $\ll k_B T$ and much longer MFPs will also be present when a temperature gradient is applied to the sample. We assert that l_M can still provide a reasonable order of magnitude estimate for this parameter's magnitude and temperature dependence, and provide for a comparison to l_λ.

With these limitations in mind, we continue our analysis by describing each magnon mode as possessing a single degree of freedom, which means that each mode transports a single quantum of heat, spin, and magnetization. This implies directly that the total magnon heat current density is proportional to the concomitant magnon spin (j_S) and magnetization (j_M) current densities; this notion can be expressed through the relationships

$$\frac{j_{Q,M}}{k_B T_M} = \frac{j_S}{\hbar} = \frac{j_M}{\mu_B}, \tag{5}$$

where T_M is the absolute magnon temperature, $\hbar$ is the reduced Planck constant, and μ_B is the Bohr magneton.

By definition, the magnon thermal mean free path l_M characterizes the typical length scale over which thermally driven magnons propagate before undergoing inelastic scattering events ("Normal" low angle elastic scattering events do not contribute to finite thermal conductivity). Vis-á-vis Eq. (5), we assert that the occurrence of inelastic magnon scattering necessarily implies the simultaneous occurrence of spin scattering. This means (within the limitations described above) that l_M becomes a useful metric for characterizing the effective distance over which thermally excited spin waves propagate in the material, i.e., the bulk thermal spin diffusion length.

In order to determine l_M experimentally, we begin with the relationship in Eq. (2). The value of κ_M can be determined by considering that both heat carriers in the material (magnons and phonons) are bosonic quasiparticles, and thus their concentrations are determined by their density of states (DOS) and the Bose-Einstein distribution function, which is itself a function of the absolute temperature. Magnons are distinct from phonons in that they result from perturbations of the magnetization, and thus they are explicitly sensitive to applied magnetic fields. This magnetic field dependence is expressed in the magnon dispersion relation, which is given for the idealized case of a Heisenberg ferromagnet by the relationship

$$\hbar\omega_k = \mu_B g_L H + D a^2 k^2, \tag{6}$$

where ω_k is the angular frequency of the magnon mode with wave vector k, g_L is the Landé factor, and H is the effective applied magnetic field. The magnon DOS is then given by [27]

$$\begin{aligned} \mathfrak{D}(\hbar\omega) &= \frac{\hbar}{4\pi^2 D^{3/2} a^3}\sqrt{\hbar\omega - \mu_B g_L H} \quad \text{if} \quad \hbar\omega > \mu_B g_L H \\ &= 0 \quad \text{if} \quad \hbar\omega < \mu_B g_L H. \end{aligned} \tag{7}$$

Applying nonzero H creates a forbidden zone in the DOS for magnons with energy $\hbar\omega < \mu_B g_L H$. By applying a sufficiently large external field to the material at a given temperature $T = \hbar\omega/k_B$, it is thus possible to create a DOS gap large enough that effectively zero magnon modes are active, and the thermal properties are then determined by phonons only. In the equivalent microscopic physical picture, magnons are suppressed when the orientations of localized spins are restricted by the applied field in such a way that the energy necessary for propagating a coherent perturbation of these spins is larger than the available thermal energy $k_B T$. For YIG, which has a Landé factor of $g_L = 2.046$, the magnon energy gap is approximately 0.14 K/kOe. This is within a suitable range such that, at low temperatures ($T \leqslant 8$ K), most magnon modes can be suppressed by the field of a superconducting magnet in the range of 70 kOe. Since this suppression falls off exponentially with temperature, it is still possible to achieve a significant reduction on the order of 20% or more at temperatures near 20 K. By freezing out the magnon contribution to the specific heat and thermal conductivity (C_M, κ_M), the effective phonon contribution to both quantities (C_λ, κ_λ) can then be determined directly, and this can be subtracted from the total specific heat or conductivity to provide an estimate for the separate magnon contribution. Combined, these quantities provide sufficient information for determining l_M and l_λ via Eq. (2) within the temperature range where magnon freeze-out can be achieved. At zero applied magnetic field, the magnon specific heat per unit volume is then

$$C_M(T) = 0.113\frac{k_B}{a^3}\left(\frac{k_B T}{D}\right)^{3/2}. \tag{8}$$

Previous studies have attempted to estimate and measure the magnetic field dependence of the thermal conductivity and specific heat of YIG crystals [28], although those efforts were focused mostly within the temperature regime below 2 K [29,30] where magnon freeze-out can be achieved with relatively small magnetic fields. One particularly insightful study was performed by Douglass [30], who measured $\kappa(H)$ from 0.5 to 4 K in fields up to 20 kOe. He observed a 70% reduction in the thermal conductivity at 0.5 K when a field of 10 kOe was applied, indicating a substantial contribution of magnons to the total thermal conductivity within this temperature range. It is important to note that extrinsic factors such as crystal quality (i.e., impurity scattering) can have a significant impact on both the magnon and phonon conductivities at low temperatures, so the absolute results of Douglass's work (as he points out) should be interpreted as sample dependent.

Douglass provided a simple estimate of the magnon thermal mean free path at 1.6 K by calculating a magnon group velocity of 3500 m/s and estimating a spin relaxation time on the order of 10^{-7}–10^{-6} s from ferrimagnetic resonance

data, which together correspond with $l_M \approx 1$ mm. However, by measuring $\kappa(H)$ directly and applying a more suitable theoretical framework, Douglass used his own experimental results to calculate the magnon thermal mean free path at 0.5 K to be approximately 100–200 microns, with the phonon mean free path approximately 130–340 microns. Since his sample dimensions were on the order of 1–5 mm, these mean free paths are still roughly an order of magnitude smaller than what would be expected if they were limited by boundary scattering alone. This suggests that the diffusive transport description remains valid in YIG even at these low temperatures, which implies the presence of defects in Douglass's crystals and/or that phonon-magnon interactions do, in fact, play an important role, even in this temperature range.

Largely inspired by this work, here we independently verify these results by measuring $\kappa(T,H)$ and $C(T,H)$, and extend them to higher applied fields and higher temperatures than Douglass was able to reach. We also interpret these results within the context of spin caloritronic phenomena such as LSSE. For clarity, we will utilize the sign convention κ_{ijk} throughout this paper, where the index i represents the direction of the applied heat current, j represents the direction along which the resulting thermal gradient was measured, and k represents the direction of the applied magnetic field. The magnon contribution to the heat capacity corresponds well to the calculated value at 2 K based on a simple Heisenberg model [13], but has a temperature dependence that is slower than the $T^{1.5}$ law predicted by that model. We will conclude that at $T >$ 5 K, the effective phonon and magnon thermal mean free paths are approximately equal. Plant [13] reports that the magnon dispersion relation becomes multibranched above about 620 GHz, corresponding to the energy of thermal magnons at 30 K. This complicates the interpretation of the spin Seebeck effect's temperature dependence in YIG [24].

II. EXPERIMENTAL PROCEDURES

Samples of single-crystal ⟨100⟩ YIG measuring $10 \times 5 \times 0.5$ mm^3 were obtained commercially (Princeton Scientific Corporation). The thermal conductivity of one crystal was measured in a Quantum Design Physical Property Measurement System (PPMS) using the Thermal Transport Option (TTO). Gold-plated copper leads and heat sinks were attached to the sample with Epotek silver epoxy, and two Cernox thermometers were used to determine the temperature of the sample at the leads. The magnetic field dependence of the Cernox thermometry was separately calibrated. Continuous thermal conductivity measurements were performed from 300 to 2 K, both at zero applied field and under a persistent field $\mathbf{H}$ of 7×10^4 Oe. This field range is well above the saturation magnetization of YIG, which is of the order 10^2 Oe [4].

Steady-state thermal conductivity measurements were also performed at a variety of temperatures and magnetic fields between $\pm 7 \times 10^4$ Oe. This measurement was conducted by applying a heat current $\mathbf{j}_Q$ along the length of the sample so as to produce a constant temperature gradient $\nabla_x T$. The magnetic field was then stepped to various values, and the whole system was allowed to reach equilibrium at each measurement condition before the thermal conductivity was recorded.

These measurements were performed in both the longitudinal [$\kappa_{xxx}(H)$, $\mathbf{H} \| \mathbf{j}_Q \| \langle 100 \rangle$] and transverse [$\kappa_{xxz}(H)$, $\mathbf{H} \perp \mathbf{j}_Q \| \langle 100 \rangle$] orientations. Since YIG adopts the cubic garnet structure, the magnetothermal conductivity is expected to be isotropic [31], which agrees with our results. When possible, κ_λ was determined in each orientation by finding the high-field saturation value of $\kappa(H)$ at each temperature point, and this value was subtracted from $\kappa(H = 0)$ to determine κ_M.

To measure the magnetic field dependence of the specific heat, a small piece of a different YIG single crystal from the same batch weighing 0.24 mg was used. Thermal grease was applied to the PPMS specific heat sample holder as an adhesive, and a calibration measurement was performed on the empty container before adding the YIG sample. The data were collected by continuously varying the temperature from 300 to 2 K, both under zero-field and applied-field (70 kOe) conditions. The value of C_M was determined by subtracting C_λ from C_{total} within the temperature and field ranges where magnon freeze-out was observed in $\kappa(T,H)$.

III. RESULTS AND DISCUSSION

The measured longitudinal (κ_{xxx}) and transverse (κ_{xxz}) thermal conductivities are shown in Figs. 1 and 2, respectively. The top frame of Fig. 1 shows the temperature dependence of the longitudinal thermal conductivity κ_{xxx}, both at zero field and at an applied field of 70 kOe. The overall behavior is typical for an electrical insulator in which the conductivity is dominated by phonons: It follows a $\sim T^3$ law at low temperatures before peaking and entering the umklapp region around 30 K, beyond which it decays following a $\sim T^{-1}$ trend. At temperatures below approximately 20 K, the applied magnetic field suppresses the conductivity by a discernible amount. The bottom frame of Fig. 1 shows a representative plot of the magnetic field dependence of κ_{xxx} (H_x) at 8 and 2 K, respectively. Figure 2 shows the same quantities for the transverse thermal conductivity κ_{xxz} as functions of temperature, both in the absence of field and at $H_z = 70$ kOe in the top frame, and conversely as a function of field at fixed temperature (2 and 8 K) in the bottom. At 2 K, we see a substantial drop in magnitude of the conductivity for relatively small fields of approximately ± 15 kOe. The conductivity appears to be constant at fields above this value, which suggests that the magnon contribution has been completely frozen out in the high-field regime. This is consistent with the expected magnon gap of $\sim$0.14 K/kOe, which predicts freeze-out at 2 K for fields of $\sim$14 kOe. However, as the temperature is further increased to 8 K, we see what appears to be incomplete magnon saturation within the range of applied fields utilized in this experiment, but still the value at 70 kOe is about 90% saturated. Overall, the results of the longitudinal (κ_{xxx}) and transverse (κ_{xxz}) conductivity measurements were not significantly different, as expected [31].

The origin of the field dependence of κ_{xxx} and κ_{xxz}, vis-à-vis Eq. (2), can be seen in Fig. 3, which shows the temperature [Fig. 3(a)] and field [Fig. 3(b)] dependence of the specific heat under the same conditions. A clear deviation between the two curves in Fig. 3(a) is seen below $\sim$15 K, indicating that the magnon modes are at least partially suppressed by the applied field within this temperature range. The degree

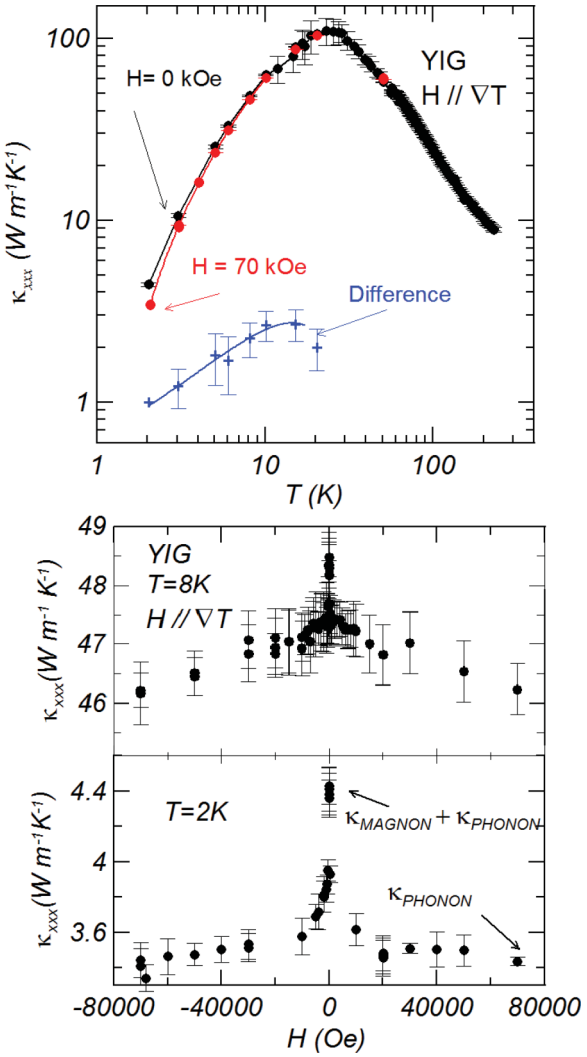

FIG. 1. (Color online) Temperature (top frame) and magnetic field (bottom frame) dependence of the thermal conductivity κ_{xxx} in the presence of a magnetic field parallel to the direction of the temperature gradient. The temperature dependence is shown in the absence of field, then in an external magnetic field of 70 kOe. In the bottom frame, the magnetic field dependence of κ_{xxx} shows a clear saturation at 2 K for applied fields of $H > 15$ kOe. At 8 K the saturation is not quite achieved even at 70 kOe, yet the saturation value is only about 2% lower than the value reached. For $T <$ 10 K, the high-field value is interpreted as arising from phonon conduction alone, while the zero-field value is interpreted as the sum of independent phonon and magnon contributions, such that the difference is the magnon thermal conductivity.

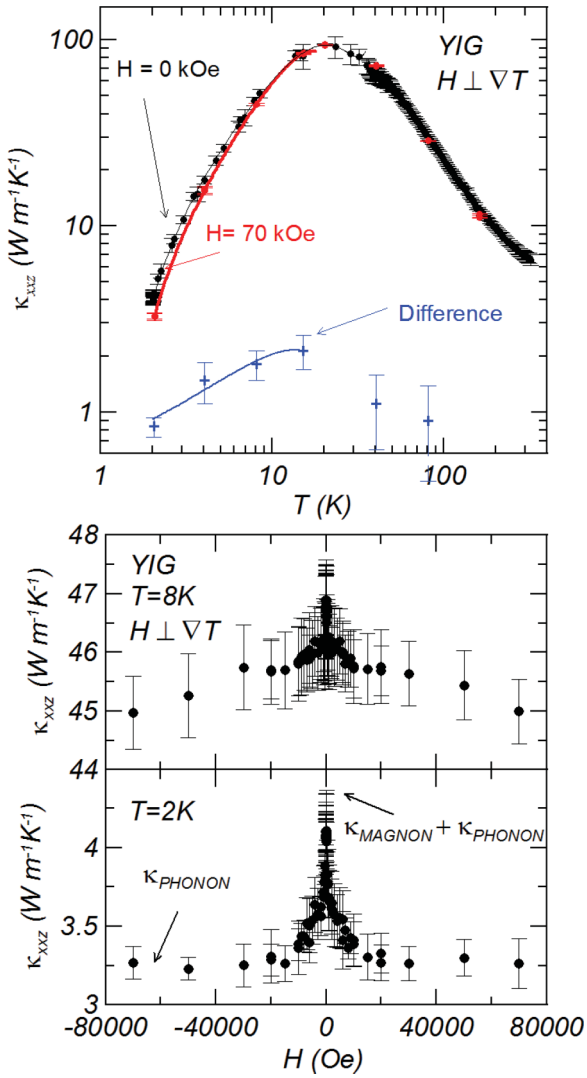

FIG. 2. (Color online) Temperature (top frame) and magnetic field (bottom frame) dependence of the transverse thermal conductivity κ_{xxz} in the presence of a magnetic field perpendicular to the direction of the temperature gradient. The description and conclusions are the same as for κ_{xxx} in Fig. 1.

of freeze-out of the magnon specific heat from the total specific heat can be evaluated from Fig. 3(b), which shows the magnetic field dependence at 3 and 8 K, respectively: At 8 K, about 90% of the magnon contribution is frozen out at 70 kOe, which also coincides with the magnon energy gap [Eq. (7)] discussed above. The estimated contributions of phonons (C_P) and magnons (C_M) from the difference between the measurements in and out of field are shown in Fig. 3(c) for the range of values in which the magnitude of the difference is larger than the associated measurement error. The dashed curve in Fig. 3(c) is calculated from Eq. (8), which assumes a parabolic dispersion relation. We obtain $D = 47$ K by fitting the data to a $T^{3/2}$ law, which corresponds quite well to the zone center value of $D = 46$ K reported in Ref. [13] from microwave measurements. In reality, the data points we report for the temperature dependence of $C_M(T)$ follow a power law that is slightly lower than $T^{3/2}$, a discrepancy we attribute to the lack of saturation of $C(H)$ at 70 kOe at higher temperature, as well as possibly to magnon-phonon interactions. We add, as an inset in Fig. 3(a), a plot of the total specific heat C represented as $CT^{-3/2}$ vs $T^{3/2}$. This plot gives the more usual way [27] for separating the magnon contribution to C_M without having to make measurements in magnetic fields. Unlike the approach used to generate the blue line in Fig. 3(c), this procedure is valid only under the assumption that Eq. (8) holds rigorously: In that case, the intercept of this plot gives the prefactor of the $T^{3/2}$ law [Eq. (8)], while the slope gives the prefactor of the Debye

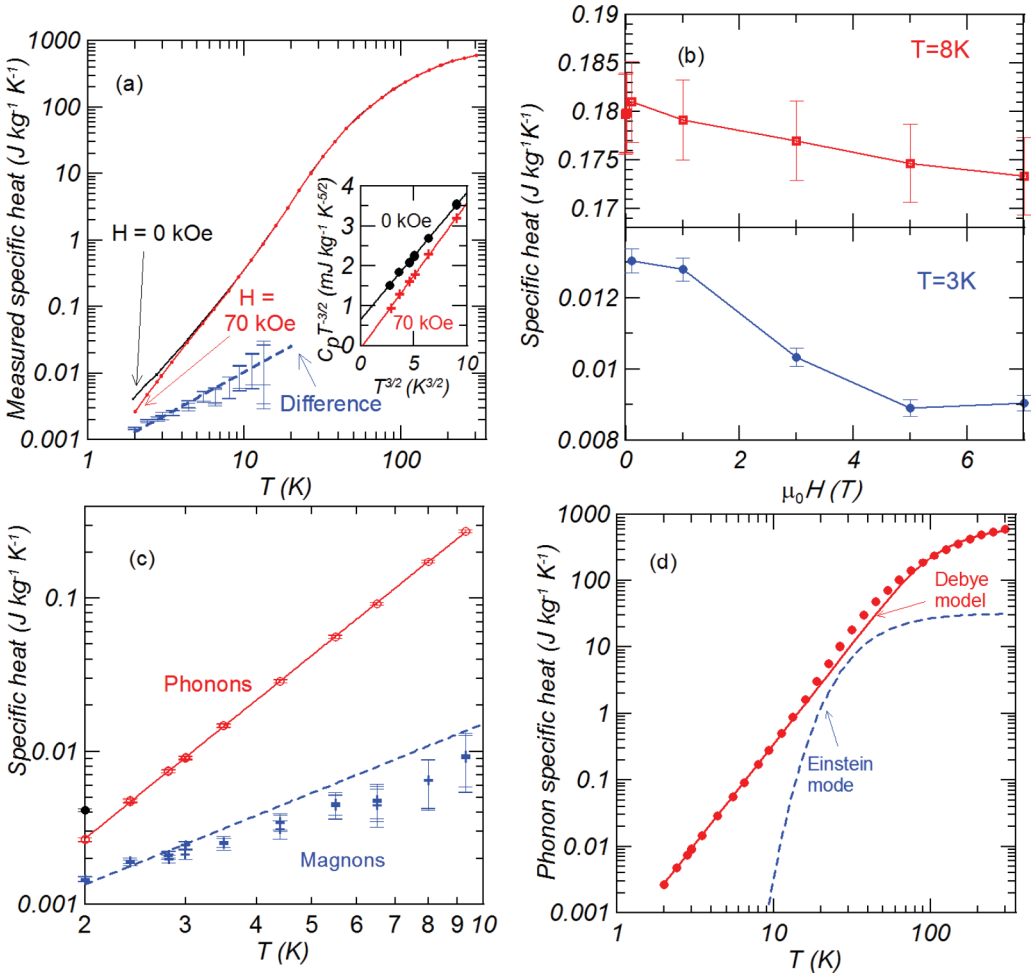

FIG. 3. (Color online) The specific heat C of YIG vs temperature (a) under constant pressure at zero magnetic field and in the presence of a 70 kOe applied external field. Inset shows the data plotted as $CT^{-3/2}$ vs $T^{3/2}$, from which the slope and intercept provide information about the phonon and magnon contributions, respectively. The magnetic field dependence of C is shown in frame (b) at two temperatures; as was the case for κ_{xxx} and κ_{xxz}, complete saturation is achieved at 2 K, but not quite at 8 K. Again, the value of C in a 70 kOe applied field is interpreted to be due to phonons (C_P), while the difference between the value in zero field and C_P is interpreted to be due to magnons (C_M) below 10 K: These are shown in (c) as a function of temperature. The dashed line is the value calculated from a simple Heisenberg model for the magnon specific heat equation (8), assuming a parabolic dispersion for magnons with a characteristic value of $D = 47$ K. The phonon specific heat is fitted in frame (d) to a Debye model (full red line) with the additional contribution of an Einstein mode (dashed blue line).

T^3 law for the phonon specific heat. For the measurements in the 70 kOe field, the intercept is approximately zero, indicating a negligible contribution from magnons. The results are thus consistent with our approach.

In Fig. 3(d) we fit the phonon specific heat $C_P(T)$ to a Debye spectrum (red line) with a Debye temperature of 531 K. An excess in C_P is visible that fits an Einstein model (blue dashed line) with an Einstein temperature of 145 K. We point out that this corresponds to the energy of an optical mode–like structure in the magnon dispersion [13], and that evidence of a magnetoelectric effect has also been reported in YIG near that temperature [32]. We do not imply at this time any causal relation between these observations, however, as the temperature is too high for us to freeze out the magnon modes with available magnetic fields.

In the range of temperatures where the magnon contribution appears to be discernibly suppressed, we can apply Eq. (3) to determine the magnon thermal mean free path, which is shown in Fig. 4 alongside the phonon thermal mean free path. To do this, we consider the group velocity for magnons with thermal energies below 30 K (i.e., those with $\hbar\omega = k_B T$) to be

$$v_M = \frac{d\omega}{dk} = 2a\sqrt{\frac{D\omega}{\hbar}} = \frac{2a}{\hbar}\sqrt{Dk_B T}. \tag{9}$$

These values range from $v_M = 3200$ m/s at 2 K to $v_M = 7100$ m/s at 10 K. For the phonon group velocity we use the average sound velocity in YIG, 4000 m/s. Both quasiparticles' thermal mean free path can be determined from either κ_{xxx} or κ_{xxz}, and the values coincide to within the experimental uncertainties. The phonon and magnon thermal mean free paths are quite similar to each other throughout the temperature range, with $l_M \approx 100$ microns at 2 K. This agrees with the magnitude of Douglass's result at the temperatures where the data overlap.

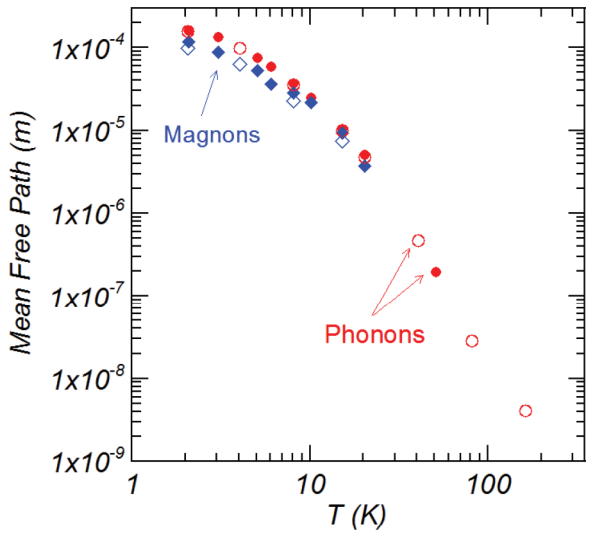

FIG. 4. (Color online) Magnon and phonon thermal mean free paths, as described by Eq. (3). The open symbols describe the results obtained from κ_{xxz} (transverse) and the full symbols those from κ_{xxx} (longitudinal) measurements, respectively. This analysis may be extended to higher temperatures if the experiment can be repeated at higher magnetic fields ($H > 15$ T), which may shed insight into the temperature dependence of magnon scattering within the phonon umklapp regime ($T > 20$ K).

IV. CONCLUSIONS

By measuring the magnetic field dependence of the thermal conductivity and specific heat of single-crystal yttrium iron garnet from 2 to 300 K, we have estimated the bulk magnon thermal mean free path within the framework of the kinetic gas theory. This value is 100 microns at 2 K, and it decreases rapidly as the temperature is increased. The magnon thermal mean free path is approximately equal to that of phonons at all temperatures reached in this experiment. This may be a direct result of magnon-phonon scattering, as the phonon mean free path also decreases rapidly ($\propto T^{-1}$) in this temperature range. As we have discussed above, this interpretation is necessarily flawed in that it produces only a single effective value for all magnon modes, and we fully expect that different modes will have different mean free paths [19]. This result is therefore only an estimate of the average length scale over which bulk spin waves travel before undergoing inelastic scattering. This estimate is conservative, especially at room temperature, where SSE experiments are typically conducted. This result therefore supports the idea discussed in Ref. [18] that high-energy bulk magnons cannot be solely or directly responsible for coherent spin transfer at the macro scale.

If we further assume that the similarity between phonon and magnon densities of states, group velocities, and Debye and Curie temperatures extends to their mean free paths, then a magnon thermal mean free path of the order of a few nanometers is expected at room temperature, much shorter than the characteristic length (150 nm) for the LSSE reported in Ref. [20]. Thermal magnons are thus expected to be in equilibrium with phonons within only a few nanometers of the interface; if these magnons are primarily responsible for LSSE, then increasing the film thickness beyond this value should have no significant effect on the LSSE signal, which is not what has been observed [20]. But if subthermal magnons are the primary drivers of SSE in YIG, which more and more evidence seems to suggest is the case, then the length scale of LSSE should be determined by the scattering length of these magnons. From this perspective, the LSSE signal would be expected to increase with film thickness until it exceeds the room temperature thermal mean free path of these modes; this may actually be the 150-nm parameter measured in the film thickness study mentioned above. Combined with our results included here, these arguments strongly suggest that the LSSE at room temperature is mediated primarily by subthermal magnons [19] with energies below about 30 or 40 K, which are the magnons that have a quadratic dispersion and do not seem to interact strongly with phonons [13]. This has been even further supported by the results of Kikkawa *et al.* [33], who reported a substantial (~30%) suppression of the LSSE signal in both YIG|Pt and YIG|Au heterostructures at room temperature when a field of ~90 kOe was applied. Since this range of fields is far too low to suppress thermal magnons at this temperature, these results also reinforce the idea that subthermal magnons constitute a disproportionately large contribution to the observed LSSE signal at all temperatures.

Nonetheless, we propose that thermal magnon modes with short wave vectors and short MFP may still be relevant for understanding and engineering thermal spin transport phenomena, in that they appear to be able to interact with both the phonon bath (via inelastic magnon-phonon scattering) and the subthermal magnon modes (via elastic magnon-magnon "Normal" interactions). We therefore suggest that the nature of magnon-magnon interactions, in addition to magnon-phonon interactions, may be an important parameter for SSE, and that further consideration should be given to the detailed spectral dependence of magnon conductivity [19].

Additional studies of the thermal properties of YIG films may provide even deeper insight into the nature of magnons, phonons, and their interactions in YIG, especially if those films are thinner than the maximum thermal mean free path we report here (~200 microns), and if the properties are measured at temperatures and fields where magnons can be frozen out. We anticipate that the thermal properties of such films will vary significantly from the behavior of the bulk sample we measured in this study, although we caution that great care should be taken to account for the detailed impact of the substrate on any thermal property measurements.

ACKNOWLEDGMENTS

This work is supported by the National Science Foundation under Grant No. CBET-1133589 and the NSF MRSEC program, Grant No. DMR 1420451.

[1] S. R. Boona, R. C. Myers, and J. P. Heremans, Energy Environ. Sci. **7**, 885 (2014).

[2] G. E. W. Bauer, E. Saitoh, and B. J. van Wees, Nat. Mater. **11**, 391 (2012).

[3] K. Uchida, S. Takahashi, K. Harii, J. Ieda, W. Koshibae, K. Ando, S. Maekawa, and E. Saitoh, Nature **455**, 778 (2008).
[4] K. Uchida, H. Adachi, T. Ota, H. Nakayama, S. Maekawa, and E. Saitoh, Appl. Phys. Lett. **97**, 172505 (2010).
[5] C. M. Jaworski, J. Yang, S. Mack, D. D. Awschalom, J. P. Heremans, and R. C. Myers, Nat. Mater. **9**, 898 (2010).
[6] J. Flipse, F. K. Dejene, D. Wagenaar, G. E. W. Bauer, J. Ben Youssef, and B. J. van Wees, Phys. Rev. Lett. **113**, 027601 (2014).
[7] E. Saitoh, M. Ieda, H. Miyajima, and G. Tatara, Appl. Phys. Lett. **88**, 182509 (2006).
[8] Y. K. Kato, R. C. Myers, A. C. Gossard, and D. D. Awschalom, Science **306**, 1910 (2004).
[9] A. Hoffmann, IEEE Trans. Magn. **49**, 5172 (2013).
[10] S. Hoffman, K. Sato, and Y. Tserkovnyak, Phys. Rev. B **88**, 064408 (2013).
[11] R. Metselaar and P. K. Larsen, Solid State Commun. **15**, 291 (1974).
[12] S. Geller and M. A. Gilleo, J. Phys. Chem. Solids **3**, 30 (1957).
[13] J. S. Plant, J. Phys. C **16**, 7037 (1983).
[14] M. Weiler, M. Althammer, M. Schreier, J. Lotze, M. Pernpeintner, S. Meyer, H. Huebl, R. Gross, A. Kamra, J. Xiao, Y.-T. Chen, H. J. Jiao, G. E. W. Bauer, and S. T. B. Goennenwein, Phys. Rev. Lett. **111**, 176601 (2013).
[15] D. J. Sanders and D. Walton, Phys. Rev. B **15**, 1489 (1977).
[16] S. Pailhès, X. Fabrèges, L. P. Régnault, L. Pinsard-Godart, I. Mirebeau, F. Moussa, M. Hennion, and S. Petit, Phys. Rev. B **79**, 134409 (2009).
[17] G. Laurence and D. Petitgrand, Phys. Rev. B **8** 2130 (1973).
[18] M. Agrawal, V. I. Vasyuchka, A. A. Serga, A. D. Karenowska, G. A. Melkov, and B. Hillebrands, Phys. Rev. Lett. **111**, 107204 (2013).
[19] K. S. Tikhonov, J. Sinova, and A. M. Finkel'stein, Nat. Commun. **4**, 1945 (2013).
[20] A. Kehlberger, R. Roeser, G. Jakob, M. Klaeui, U. Ritzmann, D. Hinzke, U. Nowak, M. C. Onbasli, D. H. Kim, C. A. Ross, M. B. Jungfleisch, and B. Hillebrands, arXiv:1306.0784.
[21] K. Uchida, J. Xiao, H. Adachi, J. Ohe, S. Takahashi, J. Ieda, T. Ota, Y. Kajiwara, H. Umezawa, H. Kawai, G. E. W. Bauer, S. Maekawa, and E. Saitoh, Nat. Mater. **9**, 894 (2010).
[22] C. W. Sandweg, Y. Kajiwara, K. Ando, E. Saitoh, and B. Hillebrands, Appl. Phys. Lett. **97**, 252504 (2010).
[23] A. Rückriegel, P. Kopietz, D. A. Bozhko, A. A. Serga, and B. Hillebrands, Phys. Rev. B **89**, 184413 (2014).
[24] K. Uchida, T. Ota, H. Adachi, J. Xiao, T. Nonaka, Y. Kajiwara, G. E. W. Bauer, S. Maekawa, and E. Saitoh, J. Appl. Phys. **111**, 103903 (2012).
[25] D. T. Morelli, J. P. Heremans, and G. A. Slack, Phys. Rev. B **66**, 195304 (2002).
[26] A. J. Minnich, J. A. Johnson, A. J. Schmidt, K. Esfarjani, M. S. Dresselhaus, K. A. Nelson, and G. Chen, Phys. Rev. Lett. **107**, 095901 (2011).
[27] C. Kittel, *Quantum Theory of Solids*, 2nd revised printing (John Wiley and Sons, New York, 1987).
[28] C. M. Bhandari and G. S. Verma, Phys. Rev. **152**, 731 (1966).
[29] B. Y. Pan, T. Y. Guan, X. C. Hong, S. Y. Zhou, X. Qiu, H. Zhang, and S. Y. Li, Europhys. Lett. **103**, 37005 (2013).
[30] R. L. Douglass, Phys. Rev. **129**, 1132 (1963).
[31] Y. C. Akgoz and G. A. Saunders, J. Phys. C **8**, 1387 (1975); **8**, 2962 (1975).
[32] Y. Kohara, Y. Yamasaki, Y. Onose, and Y. Tokura, Phys. Rev. B **82**, 104419 (2010).
[33] T. Kikkawa, K. Uchida, S. Daimon, Y. Shiomi, H. Adachi, Z. Qiu, D. Hou, X.-F. Jin, S. Maekawa, and E. Saitoh, Phys. Rev. B **88**, 214403 (2013).